


# Effect of Pore Size, Lubricant Viscosity, and Distribution on the Slippery Properties of Infused Cement Surfaces

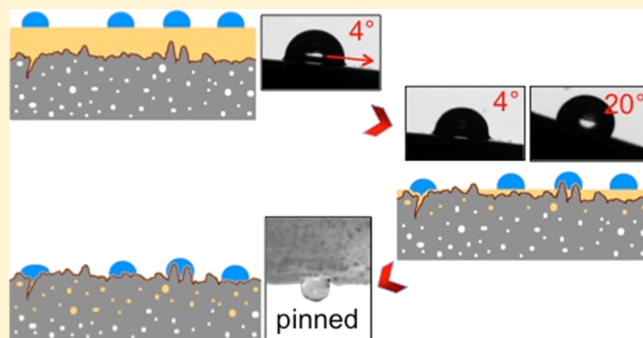
Monica Tonelli,<sup>†,‡,§</sup> Sam Peppou-Chapman,<sup>†</sup> Francesca Ridi,<sup>‡</sup> and Chiara Neto<sup>\*,†</sup> 

<sup>†</sup>School of Chemistry and University of Sydney Nano Institute, The University of Sydney, Sydney, New South Wales 2006, Australia

<sup>‡</sup>Department of Chemistry “Ugo Schiff” & CSGI, University of Florence, Sesto Fiorentino 50019, Florence, Italy

**S** Supporting Information

**ABSTRACT:** The fabrication of slippery lubricant-infused porous surfaces (SLIPS) usually requires the use of structured substrates, with specifically designed micro- and nanoroughness and complementary surface chemistry, ideally suited to trap lubricants. It is not yet established whether a random roughness, with a range of pores with a variable size reaching deep into the bulk of the material, is suitable for successful infusion. In this study, a highly porous material with random and complex roughness, obtained by using portland cement (the most common type of cementitious material), was tested for its potential to act as a SLIP surface. Atomic force microscopy meniscus measurements were used to investigate the distribution of lubricants on the surface upon subsequent stages of depletion because of the capillary absorption of the lubricant within the porous structure. Factors such as curing time of the cement paste, time since infusion, and lubricant viscosity were varied to identify the conditions under which infusion could be considered successful. A sensitive method to evaluate the penetration of liquid (low-temperature differential scanning calorimetry) was used, which could be applicable to many porous materials. The optimized infusion of cement surfaces ultimately resulted in the desired hallmarks of SLIPS, that is, high water repellence and slipperiness, effective for several weeks, reduced water permeability, and icephobicity.



## INTRODUCTION

Slippery liquid infused porous surfaces (SLIPS) are materials inspired by the slippery properties of the trumpet pitcher plant, which uses controlled surface microroughness to trap thin water films and make its pitcher slippery to insects. SLIPS have been shown to have self-cleaning,<sup>1,2</sup> anti-adhesive,<sup>3</sup> anti-icing,<sup>4–10</sup> anticorrosion,<sup>11</sup> antibiofouling,<sup>12–15</sup> and potential drag-reducing properties.<sup>11–14</sup> SLIPS are usually made of structured hydrophobic materials, where the structure is carefully controlled and optimized on the nano- and microscale, in order to obtain successful and durable infusion.<sup>13,16,17</sup> The lubricant infusion is guided by capillary wicking within the employed surface features, and therefore benefits from control over both size and surface chemistry.<sup>18</sup> For example, there is some evidence that nanoscale features are more effective than microscale features in retaining lubricants upon spinning at high rates.<sup>19</sup> Much of the research on SLIPS has focused either on fabrication methods or on the engineering aspects for specific applications. Only more recently, there have been publications which explore fundamental aspects of these materials, for example, the stability of lubricant films on surfaces with and without the structure, in air, and in the liquid to be repelled.<sup>15,20–24</sup> There still remains much work to be done to fully understand the mechanisms that underpin the function

of SLIPS. It is unclear, for example, exactly how the lubricant is displaced over time between and on top of micro- and nanostructures because of different depletion mechanisms that are likely to occur. This lack of understanding means that it is also unclear what range of surface structure is suitable for infusion, and whether real-world surfaces are likely to succeed in obtaining slippery properties.

The preparation of effective slippery liquid-infused cement surfaces has not yet been investigated, although the research on protective treatments of cement-based structures is extensive.<sup>25–28</sup> Nowadays, self-cleaning treatments on cement-based surfaces are widely used but they rely on the obtainment of hydrophobic/superhydrophobic coatings, whereas the idea that cement surfaces can be infused with silicone oils and become SLIPS, thermodynamically more stable and potentially more robust liquid-repellent surfaces,<sup>12</sup> is proposed here for the first time. SLIPS are able to prevent the adhesion of water, organic solvents, and solutions containing contaminants, including bacteria and larger marine organisms.<sup>13</sup> SLIPS are thermodynamically more stable and potentially more robust liquid-repellent surfaces than superhydrophobic ones,<sup>2,18</sup> but it

**Received:** November 19, 2018

**Revised:** January 16, 2019

72 is not obvious that the lubricant infusion could be efficiently  
73 performed on a random roughness with a high number of  
74 nanoscale and microscale pores, such as that intrinsically  
75 present in cement.

76 Here, for the first time, the porous and random structure of  
77 hardened cement paste is shown to be suited to achieve  
78 effective infusion, leading to slippery surfaces. Despite being  
79 self-assembled and somewhat uncontrolled, the characteristic  
80 micro- and nanostructure of cement surfaces does retain the  
81 lubricant as long as the curing time and infusion process are  
82 optimized for this purpose. This treatment results in high water  
83 repellence and slipperiness (as determined by low sliding  
84 angles), effective over several weeks, reduced water pene-  
85 tration, and reduction of freezing temperature of water. In this  
86 paper, a differential scanning calorimetry (DSC) method was  
87 established that allowed us to study how the degree of infusion  
88 affects the degree of penetration of water in the pores and its  
89 freezing. Moreover, calorimetry was used, for the first time, to  
90 quantitatively evaluate the icephobic properties of SLIPS-  
91 treated surfaces by looking at the temperature of ice  
92 nucleation. Infused cement surfaces not only absorb less  
93 water but they also self-clean, thus providing protection and  
94 reduced restoration costs. The conditions that underpin the  
95 stability of the infusing lubricant layer on the surface were  
96 investigated by the optimization of the infusion parameters. By  
97 performing atomic force microscopy (AFM) meniscus force  
98 measurements, the lubricant film thickness was mapped locally  
99 and over time, which was crucial in establishing the point of  
100 failure of the surfaces.

## 101 ■ MATERIALS AND METHODS

102 **Cement Paste Preparation and Characterization.** A  
103 commercial cement made by Cement Australia was used:  
104 general purpose cement type GP. This cement (up to 50% of  
105 the fresh dry material <10  $\mu\text{m}$ ) has the following composition:  
106 <97% Portland clinker, 2–5% gypsum, 0–7.5% limestone, and  
107 0–1% calcium oxide. The cement pastes here investigated were  
108 prepared with water/cement ratio = 0.4. After mixing ~20 g of  
109 cement with water for 3 min by hand, the pastes were  
110 transferred into polypropylene molds (0.5 cm diameter  $\times$  0.3  
111 cm height) and allowed to cure at room temperature. The use  
112 of molds allowed the preparation of flat reproducible samples,  
113 without affecting the physical–chemical properties of the  
114 surfaces, which are strictly related to the microstructure. Static  
115 contact angle and roll-off angle of water were measured (KSV  
116 Cam 200) at various stages before and after silanization and/or  
117 infusion, using 10  $\mu\text{L}$  droplets. The reported water static  
118 contact angle and sliding angle values are the average of at least  
119 six droplets on different regions of two samples. The hydration  
120 kinetic was monitored (DSC Q2000 calorimeter, TA Instru-  
121 ments) following a method already reported in the  
122 literature,<sup>23,24,29</sup> and is provided in the [Supporting Informa-](#)  
123 [tion](#). Surface area and pore size distribution were characterized  
124 by nitrogen gas adsorption [Coulter SA 3100, Brunauer–  
125 Emmett–Teller (BET) and Barrett–Joyner–Halenda (BJH)  
126 methods]. Pore volume percentage distribution was calculated  
127 from the adsorption curve.

128 **Surface Silanization.** A container was flushed with  
129 nitrogen gas to remove oxygen and humidity and the cement  
130 samples were placed on a Teflon base inside the container.  
131 Droplets of a volatile silane (~100  $\mu\text{L}$  of dichlorodimethylsi-  
132 lane, DCDMS, Sigma-Aldrich) were injected into the bottom  
133 of the container without touching the samples. The sealed

container was kept at room temperature for about 3 h, allowing  
silane vapor to react with the surface of the cement pastes.  
Then, the samples were washed with acetone to remove  
unbound silane.<sup>30</sup>

**Surface Infusion.** Infusion of silicone oil into samples was  
performed manually by spreading silicone oil over the surface.  
Samples were kept horizontal at room temperature. [Table 1](#)  
summarizes the information on the silicone oils used (Aldrich).

**Table 1. Different Silicone Oils Used for Infusion into the Cement Surfaces<sup>a</sup>**

viscosity of the silicone oil (cSt)	molecular weight (g)	volume used for the infusion ( $\mu\text{L}$ )
10	~1250	100
350	~14 000	100
1k	~30 000	100
10k	~63 000	40
20k	~73 000	40

<sup>a</sup>Weight average molecular weight was estimated using the Mark–Houwink correlation viscosity/molecular weight.<sup>31</sup>

**Coating Thickness.** The thickness of the 10k cSt silicone oil coating was measured at different stages via AFM meniscus force measurements (Asylum MFP-3D AFM, force mapping mode) using Multi75AL-G cantilevers (budget sensors, resonant frequency 75–80 kHz,  $k = 1–7$  N/m).<sup>16</sup>

**Water Permeability in the Porous Structure.** The permeation of water was quantified by DSC (Q2000 TA Instruments) by looking at the freezing behavior of water confined in the porous structure.<sup>32–34</sup> This method provides information on the amount of water present in different parts of the microstructure; the size of the pores in the microstructure can be distinguished based on the freezing point of the water they contain. Three cement samples at 7 days of hydration were investigated to quantify the water penetration into the pores of the cement paste. One sample was SLIPS-treated (silanised and infused with silicone oil 10k cSt) and the others were left untreated. Small pieces (milligrams) of one of the untreated sample and of the SLIPS-treated sample were separately dipped in water. After 1 day, the exterior of the samples was dried and the samples were placed in aluminum pans. An untreated sample, used as a reference, was analyzed without dipping it into water. The experiments were carried out with the following temperature program: equilibrate to 5  $^{\circ}\text{C}$ ; cooling ramp from 5 to  $-80$   $^{\circ}\text{C}$  at 0.5  $^{\circ}\text{C}/\text{min}$ ; and heating ramp from  $-80$  to  $+10$   $^{\circ}\text{C}$  at 0.5  $^{\circ}\text{C}/\text{min}$ . The water freezing peaks were integrated, and each area was used to quantify the amount of water involved, by using as standard enthalpy the estimation of  $\Delta H_0$  by Hansen et al.<sup>35</sup> at the temperature of the maximum.

**Ice Nucleation.** The cement paste was transferred in two DSC pans soon after mixing and cured at 20  $^{\circ}\text{C}$ . Then, at 7 days of hydration, one sample was silanised and infused and the other was left untreated. In both cases, a 5  $\mu\text{L}$  droplet of deionized water was added on the surface, and the pan was sealed and repeatedly cooled and thawed. To evaluate the icephobic properties of the SLIPS-treated surface in comparison with the untreated one, and taking into account the stochastic nature of nucleation of super cooled water, freeze–thawing cycles were carried out (DSC, Q2000 TA Instruments). Following a protocol reported in the literature for the study of the inhibition of ice nucleation,<sup>36,37</sup> the

183 thermal cycle was: ramp from 20 to 0 °C at 20 °C/min; ramp  
184 from 0 to -40 °C at 5 °C/min; ramp from -40 to +30 °C at  
185 20 °C/min; and equilibrate at 30 °C. In each run, the  
186 temperature at which the water froze was measured.

## 187 ■ RESULTS AND DISCUSSION

188 **Wettability.** Cement samples were prepared and allowed to  
189 cure for different times (1–40 days). Hardening of cement  
190 pastes results from the reaction between the anhydrous  
191 calcium silicates and aluminates that constitute the cement  
192 powder and water, mostly happening in the early stage of  
193 curing, which leads to the formation of an amorphous binder  
194 phase with a porous structure. Figure 1 shows a schematic of

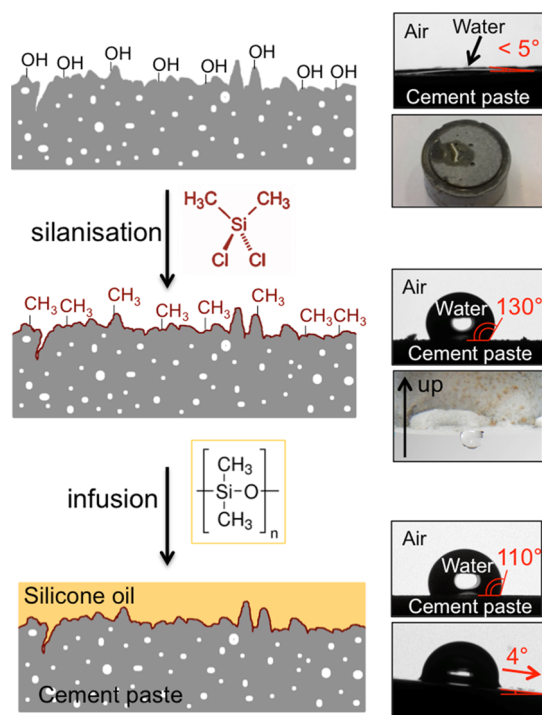


Figure 1. Schematic representation of the preparation of SLIPS based on cement with optical micrographs, showing static water contact angles and roll-off angles at each stage of surface modification.

195 the surface treatment that followed. The static water contact  
196 angle on plain cement paste surfaces was found to be  
197 consistently below  $5^\circ$ , with the water droplets becoming  
198 absorbed entirely by the surface within a few seconds of  
199 deposition. To increase the affinity of silicone oil for the  
200 cement surface under water,<sup>13</sup> the samples were hydro-  
201 phobised with DCDMS. During silanization, hydroxyl groups  
202 and hydrated species on the surface of the cement paste  
203 covalently bond the silane agents, creating a new functionalized  
204 surface with exposed  $-\text{CH}_3$  groups.<sup>30,38</sup> After silanization, the  
205 surface is hydrophobic (water contact angle around  $130^\circ$ ), but  
206 water droplets still remain pinned onto the surface (no sliding  
207 off of droplets occurred, even upon surface inversion).  
208 Following infusion with silicone oil, a hydrophobic surface is  
209 obtained (water contact angle around  $110^\circ$ ) which has slippery  
210 properties, as established based on very low watersliding angles  
211 ( $\approx 4^\circ$ ). The surfaces remained slippery to water droplets for  
212 weeks after infusion, as described below.

213 Silicone oils of different viscosities were used for the infusion  
214 of cement surfaces (at 7 days of curing), and the resulting

water-sliding angle was measured as a function of time because  
of infusion. Sliding angles were used as a qualitative measure of  
surface slipperiness, as often done in the literature.<sup>3</sup> As contact  
line pinning is a nonequilibrium process, a statistical measure  
of sliding angles is illustrated in Figure 2: a full symbol  
corresponds to >90% incidence of that sliding angle value  
being measured over at least six measurements; an empty  
symbol corresponds to <10% incidence, and the semifilled  
symbol corresponds to intermediate incidence. The values of  
water static contact angle with time are reported in Figure S1  
in the Supporting Information. The most viscous silicone oil  
used (20k cSt) produced good slippery properties, with low  
water-sliding angle values ( $<4^\circ$ ); these surfaces were also the  
most durable, with similar low sliding angle values lasting over  
periods longer than 4 weeks. Silicone oil of 10k cSt was entirely  
effective in inducing low sliding angles at short times ( $<2$   
weeks), but the sliding angles increased gradually with time.  
When using lower viscosity silicone oils (10, 350, and 1000  
cSt), water droplets pinned to the surfaces soon after infusion  
in both silanised and nonsilanised cases (sliding contact angle  
 $>180^\circ$ ). With low viscosity silicone oils, the oil was quickly  
absorbed by capillarity in the cement texture, causing the  
failure of the slippery properties (i.e. water droplets pinned  
onto the surface) after 1, 3, and 7 days when using 10, 350, and  
1000 cSt silicone oil, respectively (Figure 2A). This behavior is  
expected, as a liquid in contact with a porous material is  
absorbed by capillary forces more quickly, the less viscous the  
liquid is.<sup>28</sup> When not silanised (Figure 2B), surfaces reached  
the failure point faster, whereas the silanization treatment  
produced a more favorable infusion and, consequently, a more  
robust wettability modification with time (Figure 2A). This  
effect is particularly evident when using 10k cSt silicone oil.  
When not silanised, this sample showed a slow and gradual  
transition from a sliding angle of about  $4^\circ$  to a sliding angle  
 $>180^\circ$  at 10–17 days, during which slippery and nonslippery  
regions coexisted on the sample (Figure 2B). When silanised  
and infused, the sample showed a gradual increase of the  
sliding angle at about 2 weeks after infusion (Figure 2A, 15–16  
days). As previously observed by the authors for infused  
polymer surfaces of different chemistries,<sup>2,13</sup> hydrophobization  
of the cement is a required step for successful and robust  
infusion.<sup>39</sup>

**Treatment Optimization.** Cement-based materials have a  
complex multiscale structure that changes with curing time.  
The exact microstructure is influenced by the formation of the  
principal reaction product, calcium silicate hydrate,  $(\text{CaO})_x-$   
 $(\text{SiO}_2)_y-(\text{H}_2\text{O})$ . The aging conditions have a significant effect  
on the hydration of the cement paste and the porosity of the  
paste, which in turn strongly influence its mechanical  
properties, durability, permeability, and diffusivity.<sup>40,41</sup> As  
infusion treatments should be performed once the cement  
paste set and the microstructure has almost completely formed,  
monitoring the hydration kinetics is paramount.

Following the free water index, which is directly related to  
the degree of hydration, as a function of the time (Figure S2)  
allowed us to determine that the cement microstructure,  
because of the growing hydrated phases, was completely  
formed within less than 1 week ( $\sim 120$  h). To further  
investigate what the ideal cure time is, wettability and nitrogen  
adsorption were investigated.

Figure 3 shows the sliding angle versus time since infusion  
for a sample silanised and infused with 10k cSt silicone oil at  
different times of curing (corresponding water static contact

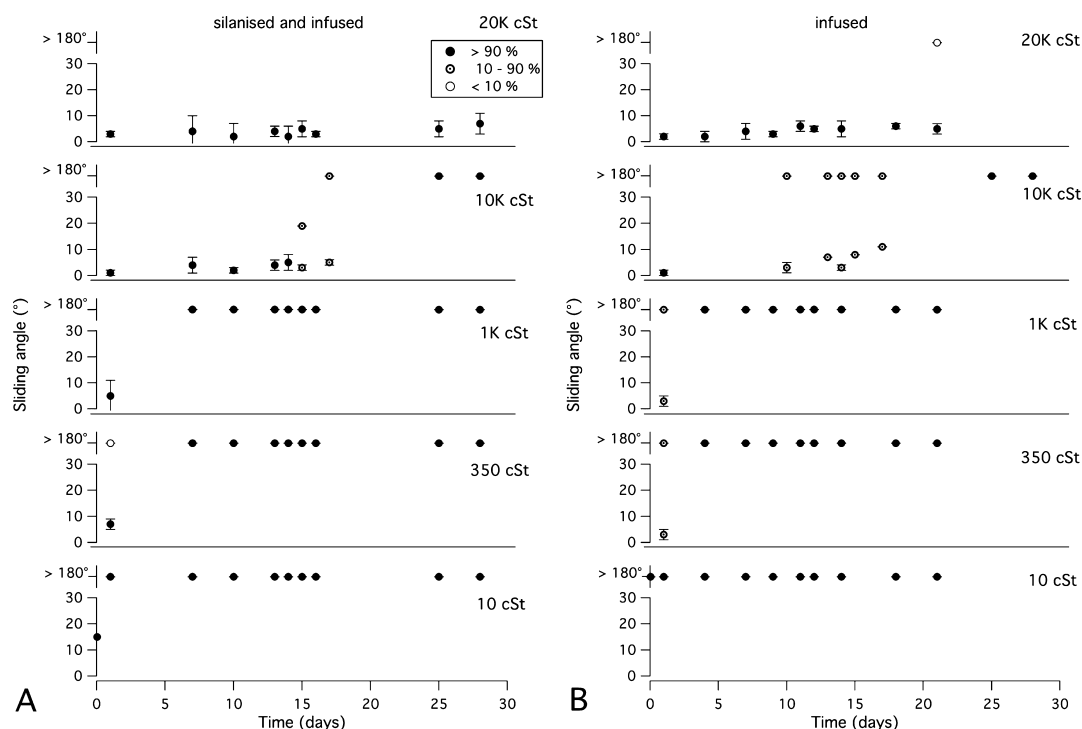


**Figure 2.** Sliding angle of a water droplet on cement surfaces over time since infusion, using silicone oils of different viscosities. (A) Cement surfaces after SLIPS treatment (silanised and infused); (B) surfaces infused without silanization. Full circles represent values measured with more than 90% incidence for that system; semi-filled circles represent values measured at between 10 and 90% incidence; and empty circles represent less than 10% incidence for that system.

278 angle reported in Figure S3). When infusion occurred after 1  
 279 day of curing of the cement paste, the system lost its slippery  
 280 properties immediately, within the first day after infusion  
 281 because of the presence of large interconnected pores in the  
 282 paste, which accelerate the drainage of the silicon oil away  
 283 from the surface and into the bulk of the cement (see nitrogen  
 284 adsorption data later). When infused after 7 or 15 days of  
 285 curing, the surfaces maintained their slippery properties for  
 286 longer times, about 2 weeks after infusion, transitioning  
 287 gradually to a hydrophobic surface onto which water droplets  
 288 remained pinned.

289 Through porosimetry, the surface area and pore size  
 290 distribution were measured at different curing times. Figure  
 291 4 shows the adsorption/desorption isotherms and the pore  
 292 volume percentage distribution for cement pastes aged 1, 7,  
 293 and 15 days, and Table 2 summarizes the BET surface area and  
 294 total pore volume calculated from the figure. All the  
 295 physisorption isotherms (Figure 4A) are compatible with  
 296 macroporous systems of type II<sup>42</sup> and the hysteresis loops can  
 297 be classified as type H3, which is associated with capillary  
 298 condensation.<sup>43</sup> The isotherms are compatible with the  
 299 existence of aggregates that give rise to polydisperse porosity  
 300 in the range from micropores to macropores (pore size >50  
 301 nm).<sup>44</sup> In cement pastes, the microstructure evolves through  
 302 the progressive closure of porosity, called depercolation  
 303 threshold, which in turn affects the transport properties that  
 304 in most degradation mechanisms govern the rate of damage.<sup>34</sup>  
 305 The hysteresis loop at 1 day of curing is very narrow, whereas  
 306 after 7 and 15 days, the pastes show a wide loop, confirming  
 307 the increase of mesopore volume that mostly occurs in the first  
 308 week. The distribution of pore size dimensions (Figure 4B)  
 309 changed over time. After 1 day of curing, a wide distribution of  
 310 pore size between 55 and 165 nm was present, together with a

population at smaller dimension, from few nanometers up to  
 311 approximately 50 nm. After 7 days, the average size of the  
 312 bigger pores markedly decreased to values centered around 90  
 313 nm, whereas the smaller population remained unaltered in  
 314 terms of dimensions but increases in terms of volume, meaning  
 315 that the number of smaller pores increased. This is because of  
 316 the progressive formation of hydrated phases that produce the  
 317 increase of the surface area and of the total pore volume (see  
 318 Table 2).<sup>34</sup> Later, at 15 days, similar pore size dimensions and  
 319 total surface area were found, with a small increase in the  
 320 number of bigger pores, which does not produce changes in  
 321 the value of the total pore volume (Table 2).  
 322

323 Considering the overall results obtained from the calorimetric  
 324 study, the wettability data, and the BET/BJH analysis, a  
 325 curing time of 7 days was considered appropriate for the  
 326 following investigations.

**Quantification of Silicone Oil on the Surface.** The  
 327 distribution of silicone oil film thickness on the infused cement  
 328 surfaces was quantified by AFM meniscus force measurements,  
 329 using a mapping technique recently developed by the  
 330 authors.<sup>16</sup> The thickness of the lubricant film present on the  
 331 surface is directly related to the antifouling and slippery  
 332 performance of SLIPS.<sup>13</sup> AFM force mapping experiments  
 333 reveal the local thickness of the lubricant with nanometric  
 334 resolution, at different stages after infusion, together with the  
 335 topography of the underlying substrate. When the tip  
 336 approaches the surface of the lubricant, there is an attractive  
 337 capillary effect, which continues as the tip moves through the  
 338 liquid. When the tip makes hard contact with the surface, a  
 339 strong repulsion is measured. The distance between the  
 340 attractive jump-in and the repulsive hard contact gives the  
 341 thickness of the lubricant while mapping the *z*-piezo position at  
 342 hard contact maps the topography.<sup>16</sup> Figure 5 shows the  
 343 15

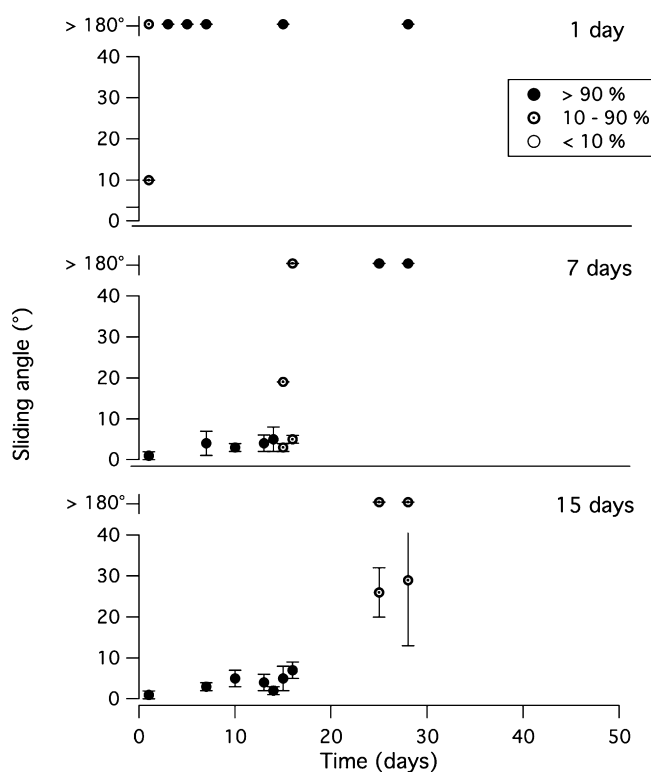


**Figure 3.** Sliding angle vs time since infusion for cement samples infused with 10k cSt silicone oil; the curing time of the cement prior to infusion is indicated in each panel. Full circles represent values measured with more than 90% incidence for that system; semifilled circles represent values measured with between 10 and 90% incidence; and empty circles represent less than 10% incidence related to the system.

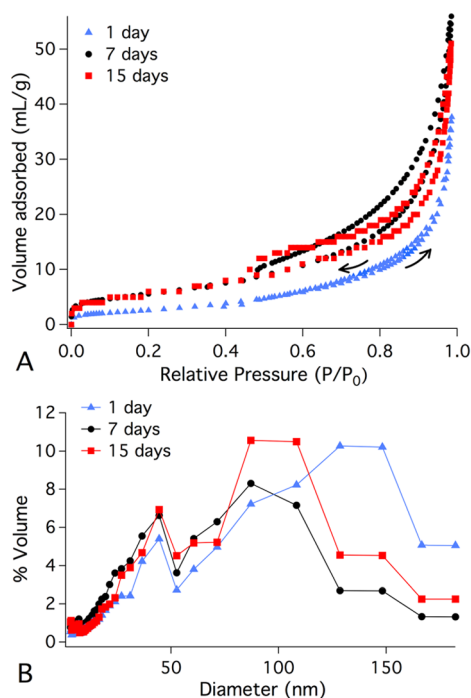


**Figure 4.** (A) Adsorption/desorption isotherms for cement samples cured for 1, 7, and 15 days; (B) distribution of pore volume percentage for cement samples at the same curing time, obtained by the BJH method.

**Table 2. BET Surface Area and BJH Pore Volume Calculated from Data in Figure 4**

curing time (day)	BET surface area (m <sup>2</sup> /g)	total pore volume (mL/g)
1	9.4	0.05
7	20.0	0.08
15	22.2	0.07

topography of a infused cement sample (part a1) and a map of 344 lubricant film thickness over the same area (part a2); the third 345 panel (a3) is the film thickness distribution over the whole 346 sample. The sample was cured for 1 week, silanised, and 347 infused with 10k cSt silicone oil, and then the meniscus force 348 measurements performed at 11, 17, and 40 days after lubricant 349 infusion. Immediately after infusion and for the first 10 days, 350 the thickness of the coating was more than 12  $\mu\text{m}$  (the 351 maximum measurable thickness, data not shown). From 11 352 days onward, a thickness of about 1–2  $\mu\text{m}$  was found (Figure 353 5A), with this situation corresponding to a highly slippery 354 surface, with a very low sliding angle (Figure 2). At 17 days 355 after infusion, the depletion became more pronounced, and 356 two populations of lubricant thickness appeared: there were 357 areas with a thickness of several hundred nm (Figure 5B) and 358 areas with lower thickness, mostly less than 200 nm (Figure 359 5C). Regions with different film thicknesses coexist, with high 360 features of the roughness becoming depleted of lubricants first. 361 These are the regions onto which the water droplets are likely 362 to remain pinned first, and, as shown in Figure 2, at this time, a 363 transition occurs from low to high values of sliding angle. 364 Depletion progressively increased over time because of the 365 absorption of the lubricant into the cement microstructure. 366 Finally, at 40 days after infusion (Figure 5D), a lubricant 367 thickness of less than 20 nm remained on the surface. Such a 368 low film thickness was not sufficient to maintain the slippery 369 properties, and indeed only high sliding angle values were 370 measured at this stage (Figure 2). The mechanism described 371 here is representative of the depletion of silicone oil occurring 372 with oils of different viscosities as well, although for higher 373 viscosity the timescale was slower (data not shown). 374

**Water Permeability.** The permeation of water in the 375 samples was monitored by low-temperature DSC, by 376 monitoring the depression of the freezing point of water 377 confined in the porous structure.<sup>33</sup> When water is constrained 378 in pores with dimensions  $\leq 1$  nm, it cannot be detected, but 379 when it is confined in larger pores, it can be quantified and 380 different populations can be distinguished: the smaller the 381 dimension of the pore, the lower the freezing temperature of 382 water confined into it.<sup>33</sup> The comparison of samples whose 383 surfaces were treated or not gives information on the effect of 384 the surface treatment on the permeation of water into the 385 microstructure. Figure 6 shows the cooling thermograms for an 386 untreated cement sample, a sample untreated and immersed 387 into water for 24 h, and a sample silanised, infused, and 388 immersed in water for 24 h. The peaks observed as the samples 389 cooled in the range  $-10$  to  $-50$   $^{\circ}\text{C}$  are due to the freezing of 390 the fraction of the water used to prepare the paste that has not 391 yet taken part in the hydration reaction and confined in pores 392 of different dimensions.<sup>32</sup> The peak at about  $-10$   $^{\circ}\text{C}$  is due to 393 the freezing of water confined in *capillary pores*, whose size is 394 large enough ( $>12$  nm) to enable the water to freeze as “bulk”, 395 unconfined water. The presence of water confined in the so- 396 called *large gel pores*, of size 3–12 nm, is revealed by the small 397 peak at about  $-25$   $^{\circ}\text{C}$ .<sup>40,45</sup> The peak at  $-40$   $^{\circ}\text{C}$  present in all 398

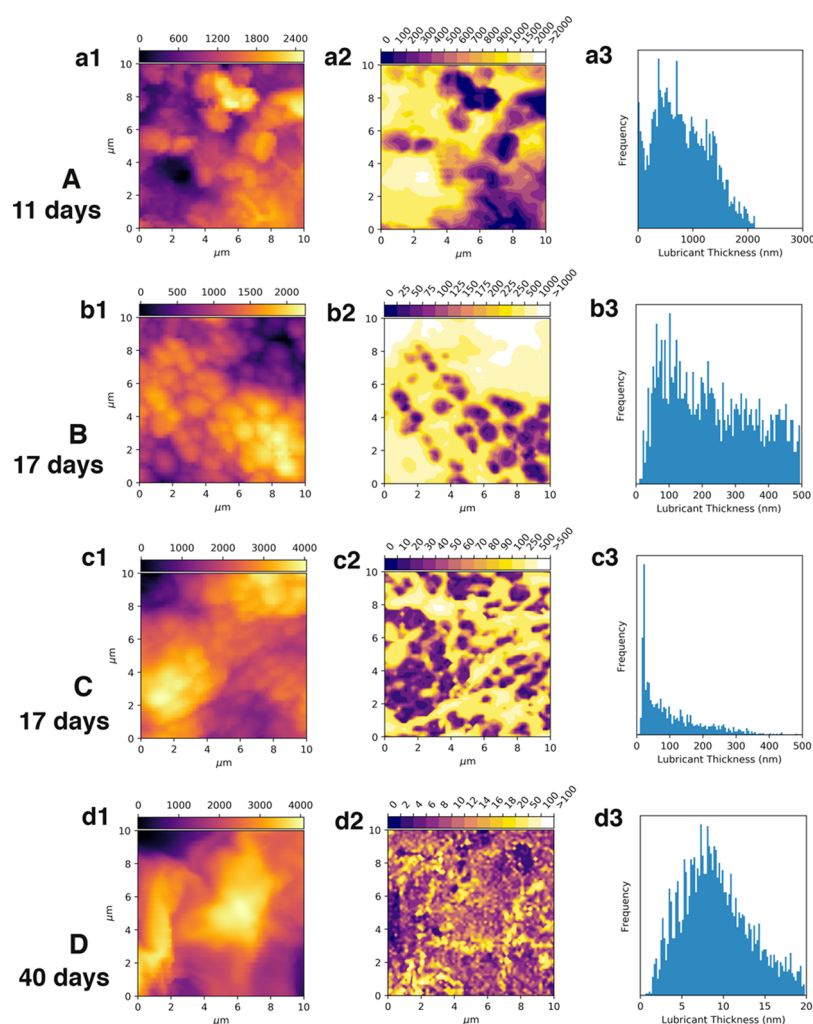


**Figure 5.** (a1–d1) Topography of cement samples; (a2–d2) map of lubricant film thickness over the same areas, measured by AFM meniscus force measurements; (a3–d3) distribution of lubricant film thickness. (A) 11, (B,C) 17, 17, and (D) 40 days.

399 the samples arises from the water confined in *small gel pores*  
 400 (1–3 nm). Each peak was integrated, and the areas were used  
 401 to calculate the amount of water involved.<sup>33</sup> The signal at –54  
 402 °C in the cooling scan of the treated sample is because of the  
 403 solidification of silicone oil, thus it was not considered.

404 **Table 3** summarizes the amount of water permeated into the  
 405 different samples. Large differences were found concerning the  
 406 capillaries: no bulklike water was found in the reference sample  
 407 and, when immersed into water, the untreated and treated  
 408 samples differ. The infused surface had a lower amount of  
 409 water confined in capillary pores than the noninfused one (7.0  
 410 vs 11.8%), which is a sign of a lower permeability. The  
 411 silanization and infusion treatment therefore reduced water  
 412 absorption in the infused cement. Nevertheless, as the test  
 413 consists of full immersion in water for 24 h, only partial water  
 414 repellence was obtained.

415 **Inhibition of Ice Nucleation.** The freeze–thaw behavior  
 416 of a water droplet onto untreated and infused cement pastes  
 417 prepared into DSC pans was investigated to establish the effect  
 418 of infusion on ice nucleation. Following a protocol reported in  
 419 the literature,<sup>46</sup> the samples were repeatedly cooled and  
 420 thawed.<sup>47</sup> The temperature at which the nucleation started was  
 421 measured from the freezing signals (Figure S4) and the  
 422 probability distribution was observed (Figure 7). The temper-  
 423 ature at which the samples froze 50% of the time ( $T_{50}$ )

represents the average nucleation temperature. **Table S1** shows  
 424 a comparison of the nucleation temperature found for the  
 425 untreated and treated samples: the presence of lubricants  
 426 significantly increased the level of supercooling from around  
 427 –9 °C for the untreated sample to –27 °C for the infused  
 428 sample (an estimate of the error in the measurement is shown  
 429 in **Table S1**). This demonstrates that infusion of the samples  
 430 imparted icephobic properties onto cement. 431

## CONCLUSIONS

432  
 433 The intrinsic roughness of cement paste was shown to be  
 434 suitable for effective trapping and infusion of silicone oil,  
 435 leading to high water repellency and slipperiness, effective for  
 436 several weeks, reduced water permeability, and icephobic  
 437 properties. The conclusions of this study are general and could  
 438 be applied to a number of porous materials where large pores  
 439 are present on the surface. Our main conclusions include:

- 440 1. The mechanism of the loss of lubricants in the cement-  
 441 like surface is mostly through penetration of the  
 442 lubricant in the bulk pore structure, through capillary  
 443 pores that reach the surface. Several approaches might  
 444 be suitable to reduce the loss of lubricants, including:  
 445 sealing the surface pores with a waxy material prior to  
 446 infusion; infusing the full volume of the porous material

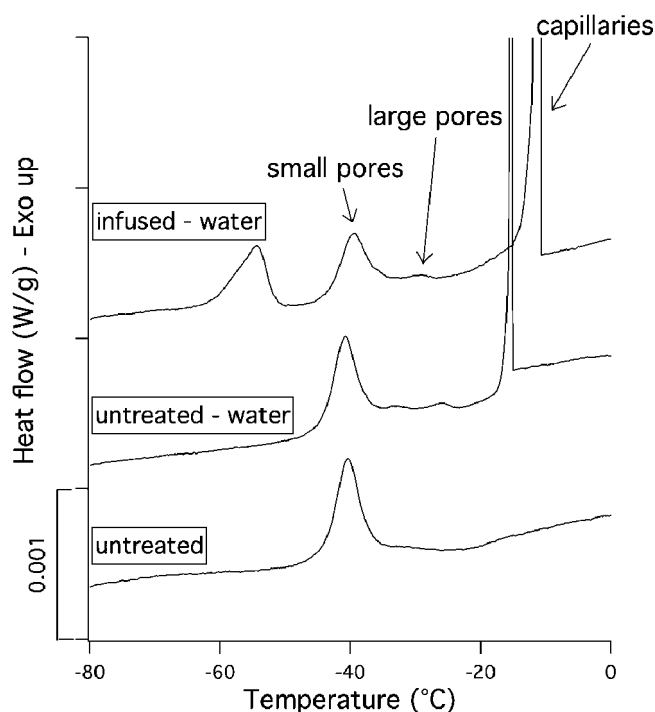


**Figure 6.** DSC thermograms of three cement pastes cured for 7 days: an untreated sample, a sample untreated and immersed in water for 24 h, and a sample infused with silicon oil and immersed in water for 24 h. The cooling scans are offset for clarity.

**Table 3. Amount of Water Freezing at Different Temperature Ranges**

sample	water amount (%) <sup>a</sup>		
	capillary pores <sup>b</sup>	large pores (3–12 nm) <sup>c</sup>	small pores (1–3 nm) <sup>d</sup>
untreated	0	0.2 ± 0.1	1.9 ± 0.5
untreated-water	11.8 ± 2.9	0.3 ± 0.1	1.8 ± 0.5
infused-water	7.0 ± 1.8	0.3 ± 0.1	1.1 ± 0.3

<sup>a</sup>The percentages are calculated with respect to the total weight of the paste. <sup>b</sup>Region of bulk-like water confined in capillaries: water freezing from  $-5$  to  $-20$  °C. <sup>c</sup>Water freezing between  $-20$  and  $-35$  °C. <sup>d</sup>Water freezing between  $-35$  and  $-50$  °C.

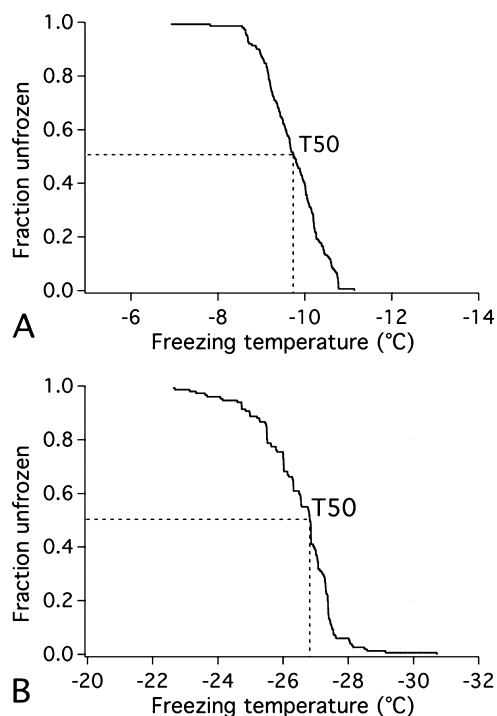


**Figure 7.** Probability distribution curves for the event of freezing for the untreated cement (A) and infused cement (B).

While low viscosity lubricants ( $<10$ k cSt) resulted in 467 poor retention of the lubricant on the cement surface, 468 because of the quick absorption in the cement porosity, 469 higher viscosity lubricants (10k and 20k cSt) resulted in 470 good slippery properties, maintained for over 4 weeks. 471

- 472 Even in surfaces with high, random, and self-assembled 473 roughness such as those studied here, the slippery 474 properties can be easily related to the amount of 475 lubricants present at each location of the surface, rather 476 than to the surface structure itself. Slippery properties 477 were observed on cement surfaces when lubricant 478 thickness was of the order of hundreds of nm. Below 479 this value of lubricant thickness, water droplets started to 480 pin on the micro- and nanoscale roughness of the 481 surface. AFM meniscus force mapping pioneered by us is 482 invaluable in relating how lubricant thickness and 483 redistribution over time affect the surface performance.
- 484 To the best of our knowledge, the permeation of water 485 into SLIPS-treated surfaces was quantified for the first 486 time by low-temperature DSC. DSC also allowed, for the 487 first time, evaluating the icephobic properties of surfaces. 488 Cement surfaces represented a case study and this 489 method is likely to be generalizable to the study of many 490 other pour material and ice nucleation on surfaces. 491 Lubricant-infused surfaces showed lower permeability 492 than noninfused ones, with the lubricant reducing water 493 absorption into capillaries. Finally, slippery cement- 494 based materials significantly lowered the freezing 495 temperature of water down to  $-27$  °C.

Given the random nature of cement roughness and the 496 presence of large pores on the surface, it is remarkable that 497 infusion was successful to this reported extent. Cement is an 498 industrially relevant material, with broad areas of interest and a 499 significant economic impact. Although further improvements 500 are necessary for the obtainment of a durable solution, this 501

447 with the lubricant (as long as the thickness of the 448 cement layer is small); and replenishing the lubricant at 449 regular (4 weeks) intervals.

450 2. The cement curing time affects the success of infusion, 451 as the pore size is highly dependent on curing time. 452 Cement surfaces needed to be cured for a minimum of 7 453 days, until the microstructure had mostly formed, before 454 infusion could be successfully conducted. At this point, 455 the highest distribution of pores was around 90 nm with 456 a smaller population of around 40 nm. The capillary 457 pores were the ones that most benefited from infusion in 458 reducing water penetration when samples were fully 459 immersed in water.

460 3. The viscosity of the lubricant affects the efficiency of 461 infusion. While in general a lower viscosity lubricant 462 naturally leads to more slippery surfaces and faster rates 463 of roll-off of droplets, in highly porous surfaces such as 464 these, higher viscosity lubricants are required, as they 465 sufficiently delay lubricant depletion via penetration into 466 the material to make the surfaces practically useful.

502 paper could contribute to develop a wide spectrum of fields,  
503 from reducing the impact of graffiti to reducing the damage by  
504 marine spray and by acid rain. This work extends the potential  
505 use of lubricant infusion to real-world materials and to surfaces  
506 with nonideal roughness.

## 507 ■ ASSOCIATED CONTENT

### 508 ● Supporting Information

509 The Supporting Information is available free of charge on the  
510 ACS Publications website at DOI: 10.1021/acs.jpcc.8b11221.

511 Water static contact angle versus time since infusion,  
512 using silicone oils of different viscosity, free water index  
513 as a function of the curing time, water static contact  
514 angle versus time since infusion for infused cement  
515 samples, freezing temperature of a water droplet onto  
516 untreated and silanised and infused samples, and  
517 comparison of water supercooling for surfaces untreated  
518 and treated (PDF)

## 519 ■ AUTHOR INFORMATION

### 520 Corresponding Author

521 \*E-mail: chiara.neto@sydney.edu.au. Phone: +61 2 9351 2752.

### 522 ORCID

523 Chiara Neto: 0000-0001-6058-0885

### 524 Present Address

525 <sup>S</sup>Department of Chemistry “Ugo Schiff” & CSGI, University of  
526 Florence, Sesto Fiorentino 50019, Florence, Italy.

### 527 Author Contributions

528 The manuscript was written through contributions of all  
529 authors. All authors have given approval to the final version of  
530 the manuscript.

### 531 Notes

532 The authors declare no competing financial interest.

## 533 ■ ACKNOWLEDGMENTS

534 The authors thank the Australian Research Council, The  
535 University of Sydney, the Consorzio Interuniversitario per lo  
536 Sviluppo dei Sistemi a Grande Interfase (CSGI) and the  
537 Erasmus Mundus NANOPHI Project for funding. Prof.  
538 Gianluca Ranzi and Osvaldo Vallati are warmly thanked for  
539 providing of the cement powders and for useful discussions.

## 540 ■ ABBREVIATIONS

541 SLIPS, slippery liquid infused surfaces; DSC, differential  
542 scanning calorimetry; BJH, Barrett–Joyner–Halenda method

## 543 ■ REFERENCES

- 544 (1) Scarratt, L. R. J.; Steiner, U.; Neto, C. A Review on the  
545 Mechanical and Thermodynamic Robustness of Superhydrophobic  
546 Surfaces. *Adv. Colloid Interface Sci.* **2017**, *246*, 133–152.  
547 (2) Owais, A.; Smith-Palmer, T.; Gentle, A.; Neto, C. Influence of  
548 Long-Range Forces and Capillarity on the Function of Underwater  
549 Superoleophobic Wrinkled Surfaces. *Soft Matter* **2018**, *14*, 6627–  
550 6634.  
551 (3) Wong, T.-S.; Kang, S. H.; Tang, S. K. Y.; Smythe, E. J.; Hatton,  
552 B. D.; Grinthal, A.; Aizenberg, J. Bioinspired Self-Repairing Slippery  
553 Surfaces with Pressure-Stable Omniphobicity. *Nature* **2011**, *477*,  
554 443–447.  
555 (4) Zhang, J.; Gu, C.; Tu, J. Robust Slippery Coating with Superior  
556 Corrosion Resistance and Anti-Icing Performance for AZ31B Mg  
557 Alloy Protection. *ACS Appl. Mater. Interfaces* **2017**, *9*, 11247–11257.

- (5) Yeong, Y. H.; Wang, C.; Wynne, K. J.; Gupta, M. C. Oil-Infused  
Superhydrophobic Silicone Material for Low Ice Adhesion with Long-  
Term Infusion Stability. *ACS Appl. Mater. Interfaces* **2016**, *8*, 32050–  
32059. 561  
(6) Kim, P.; Wong, T.-S.; Alvarenga, J.; Kreder, M. J.; Adorno-  
Martinez, W. E.; Aizenberg, J. Liquid-Infused Nanostructured  
Surfaces with Extreme Anti-Ice and Anti-Frost Performance. *ACS*  
*Nano* **2012**, *6*, 6569–6577. 565  
(7) Liu, Q.; Yang, Y.; Huang, M.; Zhou, Y.; Liu, Y.; Liang, X.  
Durability of a Lubricant-Infused Electrospray Silicon Rubber Surface  
as an Anti-Icing Coating. *Appl. Surf. Sci.* **2015**, *346*, 68–76. 568  
(8) Subramanyam, S. B.; Rykaczewski, K.; Varanasi, K. K. Ice  
Adhesion on Lubricant-Impregnated Textured Surfaces. *Langmuir*  
**2013**, *29*, 13414–13418. 571  
(9) Yin, X.; Zhang, Y.; Wang, D.; Liu, Z.; Liu, Y.; Pei, X.; Yu, B.;  
Zhou, F. Integration of Self-Lubrication and Near-Infrared Photo-  
thermogenesis for Excellent Anti-Icing/Deicing Performance. *Adv.*  
*Funct. Mater.* **2015**, *25*, 4237–4245. 575  
(10) Zhu, L.; Xue, J.; Wang, Y.; Chen, Q.; Ding, J.; Wang, Q. Ice-  
Phobic Coatings Based on Silicon-Oil-Infused Polydimethylsiloxane.  
*ACS Appl. Mater. Interfaces* **2013**, *5*, 4053–4062. 578  
(11) Wang, P.; Zhang, D.; Lu, Z.; Sun, S. Fabrication of Slippery  
Lubricant-Infused Porous Surface for Inhibition of Microbially  
Influenced Corrosion. *ACS Appl. Mater. Interfaces* **2016**, *8*, 1120–  
1127. 582  
(12) MacCallum, N.; Howell, C.; Kim, P.; Sun, D.; Friedlander, R.;  
Ranisau, J.; Ahanotu, O.; Lin, J. J.; Vena, A.; Hatton, B.; et al. Liquid-  
Infused Silicone As a Biofouling-Free Medical Material. *ACS Biomater.*  
*Sci. Eng.* **2014**, *1*, 43–51. 586  
(13) Ware, C. S.; Smith-Palmer, T.; Peppou-Chapman, S.; Scarratt,  
L. R. J.; Humphries, E. M.; Balzer, D.; Neto, C. Marine Antifouling  
Behavior of Lubricant-Infused Nanowrinkled Polymeric Surfaces. *ACS*  
*Appl. Mater. Interfaces* **2018**, *10*, 4173–4182. 590  
(14) Wang, P.; Zhang, D.; Sun, S.; Li, T.; Sun, Y. Fabrication of  
Slippery Lubricant-Infused Porous Surface with High Underwater  
Transparency for the Control of Marine Biofouling. *ACS Appl. Mater.*  
*Interfaces* **2016**, *9*, 972–982. 594  
(15) Wei, C.; Zhang, G.; Zhang, Q.; Zhan, X.; Chen, F. Silicone Oil-  
Infused Slippery Surfaces Based on Sol-Gel Process-Induced Nano-  
composite Coatings: A Facile Approach to Highly Stable Bioinspired  
Surface for Biofouling Resistance. *ACS Appl. Mater. Interfaces* **2016**, *8*,  
34810–34819. 599  
(16) Peppou-Chapman, S.; Neto, C. Mapping Depletion of  
Lubricant Films on Antibiofouling Wrinkled Slippery Surfaces. *ACS*  
*Appl. Mater. Interfaces* **2018**, *10*, 33669–33677. 602  
(17) Smith, J. D.; Dhiman, R.; Anand, S.; Reza-Garduno, E.; Cohen,  
R. E.; McKinley, G. H.; Varanasi, K. K. Droplet Mobility on  
Lubricant-Impregnated Surfaces. *Soft Matter* **2013**, *9*, 1772–1780. 605  
(18) Preston, D. J.; Song, Y.; Lu, Z.; Antao, D. S.; Wang, E. N.  
Design of Lubricant Infused Surfaces. *ACS Appl. Mater. Interfaces*  
**2017**, *9*, 42383–42392. 608  
(19) Kim, P.; Kreder, M. J.; Alvarenga, J.; Aizenberg, J. Hierarchical  
or Not? Effect of the Length Scale and Hierarchy of the Surface  
Roughness on Omniphobicity of Lubricant-Infused Substrates. *Nano*  
*Lett.* **2013**, *13*, 1793–1799. 612  
(20) Leslie, D. C.; Waterhouse, A.; Berthet, J. B.; Valentin, T. M.;  
Watters, A. L.; Jain, A.; Kim, P.; Hatton, B. D.; Nedder, A.; Donovan,  
K.; et al. A Bioinspired Omniphobic Surface Coating on Medical  
Devices Prevents Thrombosis and Biofouling. *Nat. Biotechnol.* **2014**,  
*32*, 1134–1140. 617  
(21) Yuan, S.; Li, Z.; Song, L.; Shi, H.; Luan, S.; Yin, J. Liquid-  
Infused Poly(styrene-*b*-isobutylene-*b*-styrene) Microfiber Coating  
Prevents Bacterial Attachment and Thrombosis. *ACS Appl. Mater.*  
*Interfaces* **2016**, *8*, 21214–21220. 621  
(22) Manabe, K.; Kyung, K.-H.; Shiratori, S. Biocompatible Slippery  
Fluid-Infused Films Composed of Chitosan and Alginate via Layer-by-  
Layer Self-Assembly and Their Antithrombogenicity. *ACS Appl.*  
*Mater. Interfaces* **2015**, *7*, 4763–4771. 625



- 626 (23) Damasceni, A.; Dei, L.; Fratini, E.; Ridi, F.; Chen, S.-H.;  
627 Baglioni, P. A Novel Approach Based on Differential Scanning  
628 Calorimetry Applied to the Study of Tricalcium Silicate Hydration  
629 Kinetics†. *J. Phys. Chem. B* **2002**, *106*, 11572–11578.
- 630 (24) Ridi, F.; Dei, L.; Fratini, E.; Chen, S.-H.; Baglioni, P. Hydration  
631 Kinetics of Tri-Calcium Silicate in the Presence of Superplasticizers. *J.*  
632 *Phys. Chem. B* **2003**, *107*, 1056–1061.
- 633 (25) Muhammad, N. Z.; Keyvanfar, A.; Majid, M. Z. A.; Shafaghat,  
634 A.; Mirza, J. Waterproof Performance of Concrete: A Critical Review  
635 on Implemented Approaches. *Constr. Build. Mater.* **2015**, *101*, 80–90.
- 636 (26) Han, B.; Zhang, L.; Ou, J. Hydrophobic/Superhydrophobic  
637 Concrete. *Smart and Multifunctional Concrete Toward Sustainable*  
638 *Infrastructures*; Springer Singapore: Singapore, 2017; pp 339–357.
- 639 (27) Wittmann, F. H.; Wittmann, A. D. A.; Wang, P. G. Capillary  
640 Absorption of Integral Water Repellent and Surface Impregnated  
641 Concrete. *Restor. Build. Monum.* **2014**, *20*, 281–290.
- 642 (28) de Vries, I. J.; Polder, R. B. Hydrophobic Treatment of  
643 Concrete. *Constr. Build. Mater.* **1997**, *11*, 259–265.
- 644 (29) Ridi, F.; Fratini, E.; Luciani, P.; Winnefeld, F.; Baglioni, P.  
645 Hydration Kinetics of Tricalcium Silicate by Calorimetric Methods. *J.*  
646 *Colloid Interface Sci.* **2011**, *364*, 118–124.
- 647 (30) Sagiv, J. Organized Monolayers by Adsorption. 1. Formation  
648 and Structure of Oleophobic Mixed Monolayers on Solid Surfaces. *J.*  
649 *Am. Chem. Soc.* **1980**, *102*, 92–98.
- 650 (31) Gotz, J.; Weisser, H. Correlation of the Viscosity and the  
651 Molecular Weight of Silicone Oils with the  $T_2$  NMR Relaxation  
652 Times. *Organosilicon Chemistry V*; Wiley, 2008; pp 584–594.
- 653 (32) Ridi, F.; Fratini, E.; Luciani, P.; Winnefeld, F.; Baglioni, P.  
654 Hydration Kinetics of Tricalcium Silicate by Calorimetric Methods. *J.*  
655 *Colloid Interface Sci.* **2011**, *364*, 118–124.
- 656 (33) Ridi, F.; Luciani, P.; Fratini, E.; Baglioni, P. Water Confined in  
657 Cement Pastes as a Probe of Cement Microstructure Evolution. *J.*  
658 *Phys. Chem. B* **2009**, *113*, 3080–3087.
- 659 (34) Ridi, F.; Fratini, E.; Baglioni, P. Fractal Structure Evolution  
660 during Cement Hydration by Differential Scanning Calorimetry:  
661 Effect of Organic Additives. *J. Phys. Chem. C* **2013**, *117*, 25478–  
662 25487.
- 663 (35) Hansen, E. W.; Gran, H. C.; Sellevold, E. J. Heat of Fusion and  
664 Surface Tension of Solids Confined in Porous Materials Derived from  
665 a Combined Use of NMR and Calorimetry. *J. Phys. Chem. B* **1997**,  
666 *101*, 7027–7032.
- 667 (36) Wilson, P. W.; Heneghan, A. F.; Haymet, A. D. J. Ice  
668 Nucleation in Nature: Supercooling Point (SCP) Measurements and  
669 the Role of Heterogeneous Nucleation. *Cryobiology* **2003**, *46*, 88–98.
- 670 (37) Heneghan, A. F.; Wilson, P. W.; Haymet, A. D. J.  
671 Heterogeneous Nucleation of Supercooled Water, and the Effect of  
672 an Added Catalyst. *Proc. Natl. Acad. Sci. U.S.A.* **2002**, *99*, 9631–9634.
- 673 (38) Stewart, A.; Schlosser, B.; Douglas, E. P. Surface Modification  
674 of Cured Cement Pastes by Silane Coupling Agents. *ACS Appl. Mater.*  
675 *Interfaces* **2013**, *5*, 1218–1225.
- 676 (39) Daniel, D.; Timonen, J. V. I.; Li, R.; Velling, S. J.; Aizenberg, J.  
677 Oleoplaning Droplets on Lubricated Surfaces. *Nat. Phys.* **2017**, *13*,  
678 1020–1025.
- 679 (40) Jennings, H. M. Refinements to Colloid Model of C-S-H in  
680 Cement: CM-II. *Cem. Concr. Res.* **2008**, *38*, 275–289.
- 681 (41) Pane, I.; Hansen, W. Investigation of Blended Cement  
682 Hydration by Isothermal Calorimetry and Thermal Analysis. *Cem.*  
683 *Concr. Res.* **2005**, *35*, 1155–1164.
- 684 (42) Giles, C. H.; Smith, D.; Huitson, A. A general treatment and  
685 classification of the solute adsorption isotherm. I. Theoretical. *J.*  
686 *Colloid Interface Sci.* **1974**, *47*, 755–765.
- 687 (43) Sing, K. S. W.; Everett, D. H.; Haul, R. A. W.; Moscou, L.;  
688 Pierotti, R. A.; Rouquerol, J.; Siemieniewska, T. Reporting  
689 Physisorption Data for Gas/Solid Systems. *Pure Appl. Chem.* **1985**,  
690 *57*, 603–619.
- 691 (44) Thommes, M.; Kaneko, K.; Neimark, A. V.; Olivier, J. P.;  
692 Rodriguez-Reinoso, F.; Rouquerol, J.; Sing, K. S. W. Physisorption of  
693 Gases, with Special Reference to the Evaluation of Surface Area and  
Pore Size Distribution (IUPAC Technical Report). *Pure Appl. Chem.* **694**  
**2015**, *87*, 1051–1069. 695
- (45) Jennings, H. M.; Bullard, J. W.; Thomas, J. J.; Andrade, J. E.; 696  
Chen, J. J.; Scherer, G. W. Characterization and Modeling of Pores 697  
and Surfaces in Cement Paste. *J. Adv. Concr. Technol.* **2008**, *6*, 5–29. 698
- (46) Wilson, P. W.; Lu, W.; Xu, H.; Kim, P.; Kreder, M. J.; 699  
Alvarenga, J.; Aizenberg, J. Inhibition of Ice Nucleation by Slippery 700  
Liquid-Infused Porous Surfaces (SLIPS). *Phys. Chem. Chem. Phys.* **701**  
**2013**, *15*, 581–585. 702
- (47) Monteilhet, L.; Korb, J.-P.; Mitchell, J.; McDonald, P. J. 703  
Observation of Exchange of Micropore Water in Cement Pastes by 704  
Two-Dimensional T<sub>2</sub> – T<sub>2</sub> Nuclear Magnetic Resonance 705  
Relaxometry. *Phys. Rev. E: Stat., Nonlinear, Soft Matter Phys.* **2006**, 706  
*74*, 061404. 707